The Mechanism for Unimolecular Decomposition of RDX (1,3,5-Trinitro-1,3,5-triazine), an ab Initio Study

Debashis Chakraborty, Richard P. Muller, Siddharth Dasgupta, and William A. Goddard, III*

Materials and Process Simulation Center, Beckman Institute (139-74), Division of Chemistry and Chemical Engineering, California Institute of Technology, Pasadena, California 91125

Received: October 18, 1999

Gas phase hexahydro-1,3,5-trinitro-1,3,5-triazine (RDX) is a relatively stable molecule which releases a large amount of energy upon decomposition. Although gas-phase unimolecular decomposition experiments suggest at least two major pathways, there is no mechanistic understanding of the reactions involving RDX or other energetic molecules (such as HMX and TATB), used in applications ranging from automobile air bags to rocket propellants. For the unimolecular decomposition of RDX, we find three pathways: (i) *concerted decomposition* of the ring to form three CH_2NNO_2 ($M = 74$) molecules, and (ii) *homolytic cleavage* of an NN bond to form NO_2 ($M = 46$) plus RDR ($M = 176$), which subsequently decomposes to form various products. Experimental studies suggest that the concerted pathway is dominant while theoretical calculations have suggested that the homolytic pathway might require significantly less energy. We report here a third pathway: (iii) successive *HONO elimination* to form 3 HONO ($M = 47$) plus stable 1,3,5-triazine (TAZ) ($M = 81$) with subsequent decomposition of HONO to HO ($M = 17$) and NO ($M = 30$) and at higher energies of TAZ into three HCN ($M = 27$). We examined all three pathways using first principles quantum mechanics (B3LYP, density functional theory), including the barriers for all low-lying products. We find: A threshold at ∼40 kcal/mol for which *HONO elimination* leads to TAZ plus 3 HONO, while *NN homolytic* cleavage leads to RDR plus NO_2, and the *concerted pathway* is not allowed; above ∼52 kcal/mol the TAZ of the HONO elimination pathway can decompose into 3 HCN while the HONO can decompose into HO + NO; above ∼60 kcal/mol the concerted pathway opens to form CH_2NNO_2; at a threshold of ∼65 kcal/mol the RDR of the NN homolytic pathway can decompose into other products. These predictions are roughly consistent with previous experimental results and should be testable with new experiments. This should aid the development of a kinetic scheme to understand combustion and decomposition of solid-phase RDX and related energetic compounds (e.g., HMX).

I. Introduction

The cyclic nitramines hexahydro-1,3,5-trinitro-1,3,5-triazine (RDX) and octahydro-1,3,5,7- tetranitro-1,3,5,7-tetrazocine (HMX), are important energetic ingredients for various propellants and explosives since they release a large amount of energy in bulk decomposition. Thermal decomposition of these energetic materials has been observed to form very simple final product molecules, such as HCN, NO, N_2O, NO_2, CO, CO_2, H_2O, H_2CO, etc. Understanding the underlying complex chemical processes is essential to obtain an improved model for combustion or detonation of these energetic materials.

A number of experimental studies[1−20] have been directed toward elucidating the mechanistic details of the thermal decomposition of RDX, and various *plausible* reaction pathways have been proposed. Many experiments dealt with bulk phase materials,[1−13] including decomposition in the condensed phase (solid or liquid) and the gas-phase flame structure near the burning RDX surface. The results reported have varied widely depending on the experimental conditions. To determine the initial steps of decomposition for these condensed phase studies, we focused on the gas-phase pyrolysis.

I.A. Experimental Studies. In an effort to understand the molecular level decomposition mechanism of RDX, Zhao, Hinsta, and Lee (ZHL), studied the infrared multiphoton dissociation (IRMPD) of RDX in a molecular beam using a time-of-flight velocity spectra (TOFVS).[16] They detected mass fragments of 120, 102, 81, 74, 56, 46, 44, 42, 26−30, and 12−17 as the major products from laser photolysis (which includes mass fragments of both primary and secondary decomposition products). ZHL concluded that the dominant primary channel in the RDX decomposition is a concerted symmetric triple fission of RDX ring. Based on the reported heat of formation of 33.6 kcal/mol for methylenenitramine (MN) by Melius and Binkley,[21] ZHL estimated the endothermicity to be 80 kcal/mol for the concerted ring fission (which compares with the N−N bond dissociation energy of 48 kcal/mol calculated by Melius and Binkley). ZHL estimated that the laser pulse in their experiments deposited a total internal energy of 80 kcal/mol. Thus, they concluded "the concerted ring breaking is energetically accessible for a large fraction of the RDX in this experiment, even though the endoergicity derived from the heat of formation of MN given by Melius and Binkley seems *un*reasonably high".

On the other hand, more recent UV photolysis experiments[18−20] observed N−NO_2 homolysis as the primary decomposition reaction.

Behrens and Bulusu[2] using simultaneous thermogravimetry modulated beam mass spectrometry measurements, TOFVS

analysis and isotopic crossover experiments suggested formation of oxy-s-triazine (OST) via the elimination of an HNO and two HONO molecules in the unimolecular decomposition of RDX in addition to other decomposition products. They concluded that OST is the only decomposition product from RDX that solely exhibits unimolecular decomposition kinetics. The rate of formation of OST has a first-order deuterium kinetic isotope effect which supports the HONO elimination as the rate-controlling step.

Moreover, Capellos et al.[17] based on photodissociation of RDX using 248 nm radiation (KrF laser) considered that concerted HONO elimination through a five-member cyclic transition state (TS) is the most likely primary decomposition pathway.

In addition, formation of N_2O_4 was observed in the CO_2 laser pyrolysis of RDX thin films.[18] This result was interpreted mechanistically as $N-NO_2$ cleavage followed by dimerization of NO_2 radical.

Recently, CO_2 laser-induced pyrolysis of RDX,[12] identified 47, 54, 56, 70, 81, and 97 as the parent mass fragments below m/e 100 in addition to the usual small mass fragments (18, 27, 30, 44, 46).

Summarizing, there is experimental evidence for both the concerted and N−N homolysis dissociation pathways.

I.B. Theoretical Studies. The first qualitative theoretical analysis of the decomposition mechanism for RDX (Melius and Binkley[21]) used ab initio quantum mechanics at the MP4 level, corrected empirically (BAC-MP4). The conclusion was that the N−N homolytic cleavage is the primary decomposition pathway. Assuming RDX has $N-NO_2$ bond dissociation energy similar to nitramine and methyl nitramine, they estimated a dissociation energy of ~48 kcal/mol for RDX.

Harris and Lammertsma[22] and Rice and Chabalowski[23] reported detailed studies of the conformations and bond dissociation energies of RDX using ab initio (MP2) and density functional (DFT-B3LYP) methodologies. They suggested that several conformational minima for RDX exist within a small energy range of about 1 kcal/mol. Furthermore, Harris and Lammertsma concluded that the $N-NO_2$ and C−H bonds in RDX are unusually weak, indicating that the initiation of decomposition by N−N bond cleavage and propagation of the decomposition by H atom transfer should be facile.

Sewell and Thompson[24] used classical dynamics to study RDX decomposition. They estimated that the barrier height for the concerted ring breaking is 37 kcal/mol (based on available thermochemical information in the literature), confirming the experimental interpretation of ZHL.[16] Later a similar study by Chambers and Thompson[25] demonstrated that a concerted barrier height of <40 kcal/mol is required to establish the branching ratio observed by ZHL.

Habibollazadeh et al.[26] carried out calculations at the semiempirical, ab initio, and DFT-LDA (local density approximation) level. They concluded that the barrier for the concerted fission is 72−75 kcal/mol.

Recently, Wu and Fried[27] carried out an extensive series of high-level DFT calculations (B3LYP, B3PW91, BPW91) of the potential energy profile for two dissociation channels: (I) $N-NO_2$ bond rupture and (II) concerted ring fission to three MN molecules. They found that path I is favored by 18.3 kcal/mol over II, suggesting that $N-NO_2$ bond rupture is the dominant channel in gas-phase decomposition of RDX.

Summarizing, these theoretical studies have provided support for both the concerted and N−N homolytic fission pathways, but somewhat favors the latter.
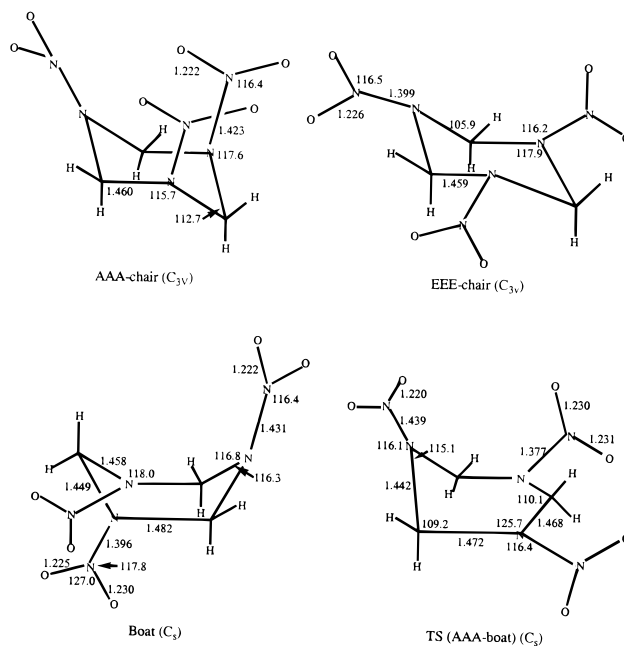

Figure 1. Optimized geometries of RDX in the AAA chair, EEE chair, and boat conformations and the corresponding boat to AAA chair transition state.

I.C. Current Work. Despite the large number of experimental and theoretical investigations, the mechanism of thermal decomposition of RDX is still uncertain. Experimentalists have observed numerous products in the thermal decomposition of RDX and have suggested two plausible qualitative schemes.[13] Most theoretical calculations have been restricted to either conformational analysis of RDX or validation of the ZHL observations. Thus, they have considered just the two initial decomposition pathways, concerted ring fission versus N−N bond cleavage. Consequently, we decided to carry out a detailed mechanistic study of thermal decomposition of RDX using ab initio DFT methodology (B3LYP).

Section II outlines the computational methods while Section III presents the calculational results. These are compared to experiment in Section IV, with the summary in Section V.

II. Computational Methods

The geometries of the reactants, products, intermediates, and transition states (TS) have been optimized at the B3LYP flavor of density functional theory. This includes the generalized gradient approximation (Becke 1988 nonlocal gradient correction), exact exchange using the Becke three parameter exchange functional,[28] and the nonlocal correlation functional of Lee, Yang, and Parr.[29] We used the modest 6-31G(d) basis set to be consistent with practical extensions of the same level of calculation to higher analogue such as HMX. This level of theory is expected to predict the energetics of large molecular systems such as RDX to a few kcal/mol.[22,27]

All stationary points have positively identified for local minima [number of imaginary frequencies (NIMAG) = 0] and for TS (NIMAG = 1). Vibrational frequencies were calculated at all stationary points to obtain zero-point energies (ZPE) and thermodynamic parameters. All calculations were carried out with Jaguar quantum chemistry program package.[30]

III. Results

Figure 1 shows the optimized geometry of RDX in two different conformations (chair and boat) and the corresponding
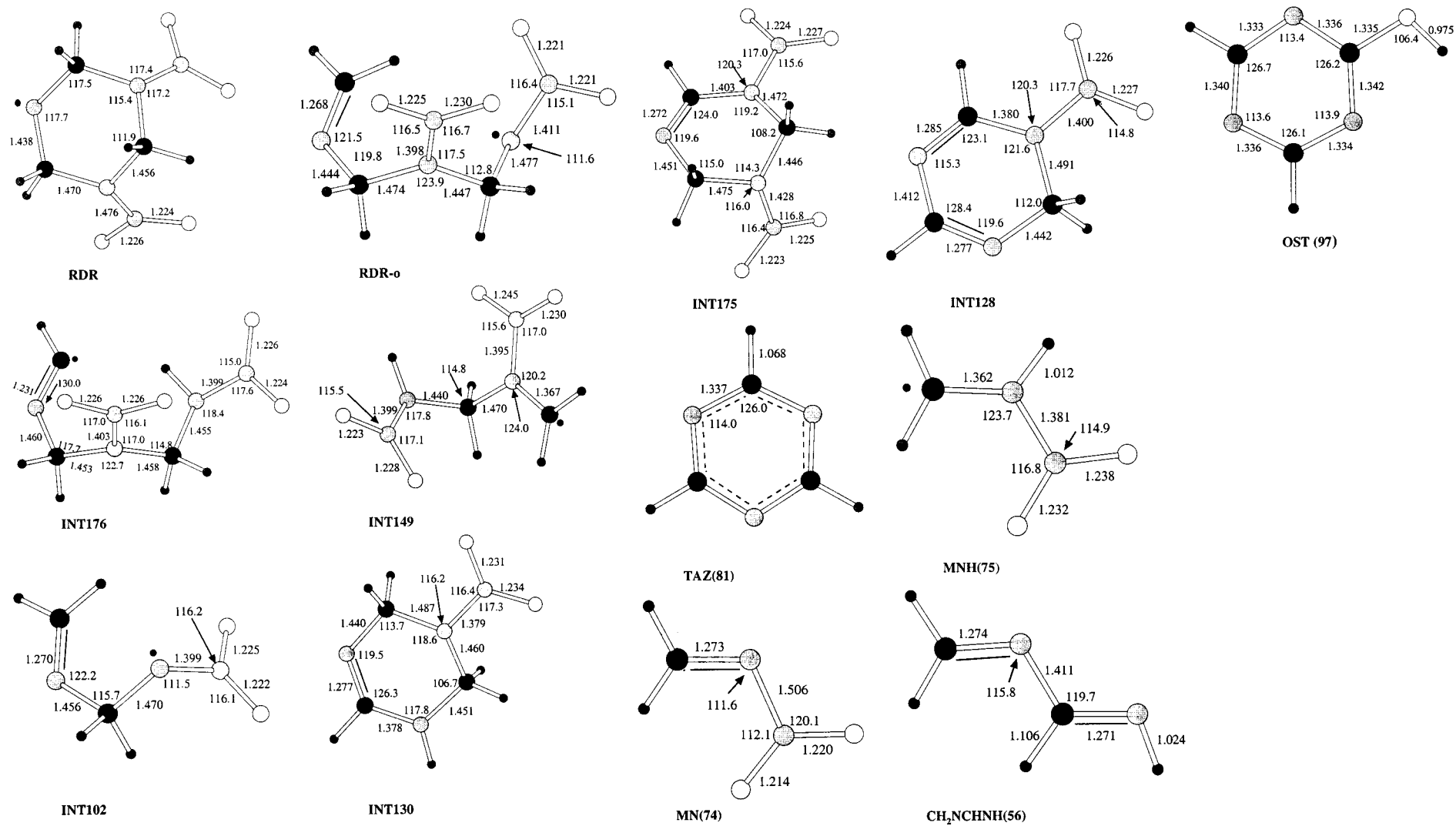
Figure 2. Optimized structures of the intermediates and some important products in the unimolecular decomposition of RDX. Symbols ●○○• represent the C, N, O and H atoms, respectively.
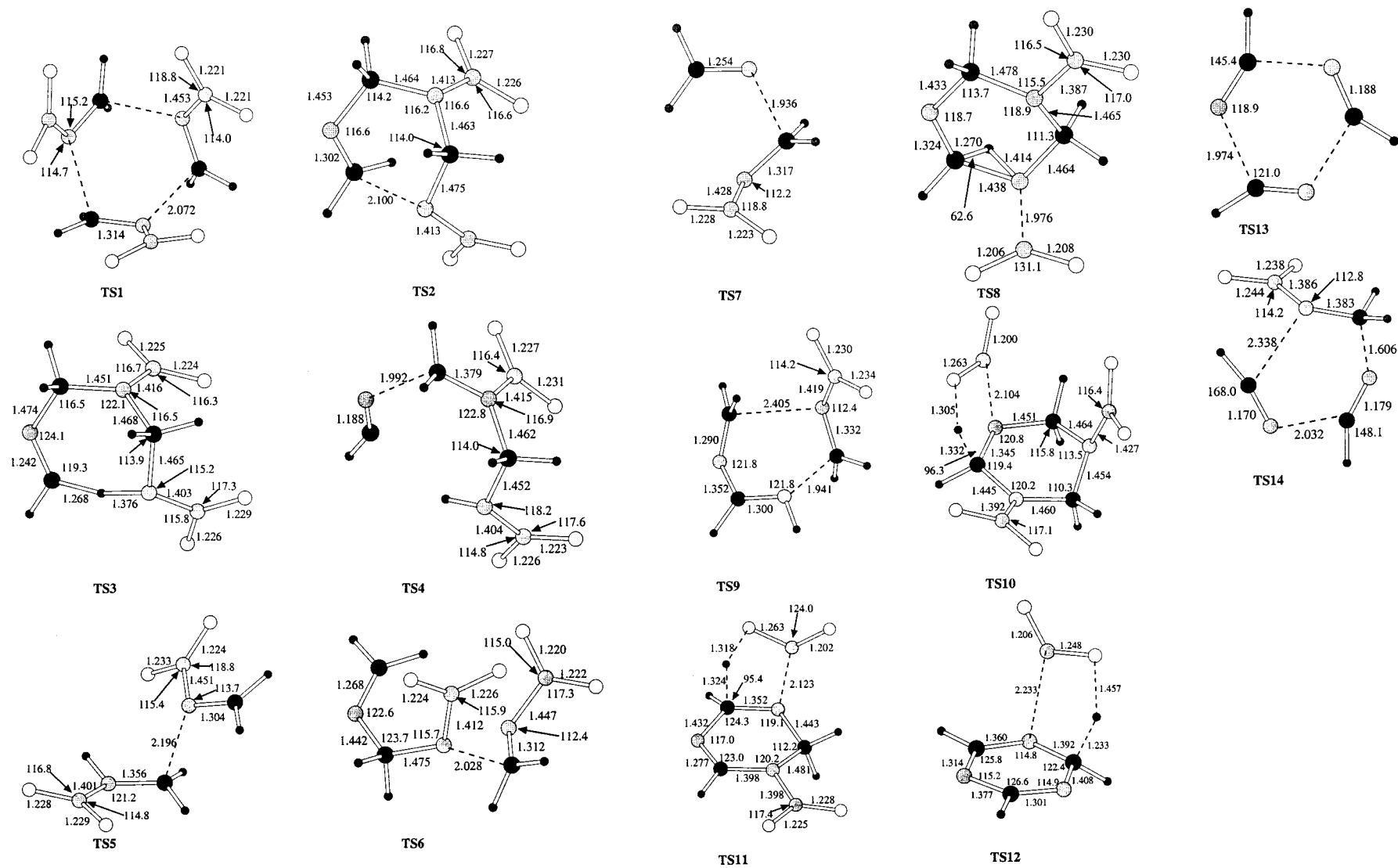
Figure 3. Optimized structure of the transition states in the unimolecular decomposition of RDX. Symbols ●○○• stands for C, N, O, and H atoms, respectively.

TABLE 1: Calculated Frequencies of the Transition States at the B3LYP/6-31G(d) Level of Theory[a]

TS1

−397	23	32	32	74	74	77	132	133	176	190	190	380	381	404
408	409	454	587	587	595	655	657	657	736	740	741	840	840	867
935	937	940	1067	1114	1114	1193	1205	1205	1311	1311	1335	1363	1389	1389
1523	1543	1544	1670	1694	1694	3163	3163	3164	3265	3265	3266			

TS2

−567	54	67	81	99	179	249	276	321	354	411	450	511	547	599
637	708	761	762	811	858	873	934	946	971	999	1039	1114	1168	1187
1273	1295	1330	1348	1358	1385	1431	1472	1487	1558	1623	1658	3052	3065	3094
3107	3174	3212												

TS3

−1392	56	66	79	106	123	244	278	326	355	420	429	491	529	599
614	656	698	749	765	779	856	881	899	925	985	1049	1126	1147	1210
1226	1304	1323	1344	1347	1380	1410	1467	1488	1538	1635	1673	1813	3085	3092
3116	3174	3184												

TS4

−604	49	58	71	90	103	117	159	220	254	333	414	429	445	542
594	602	615	629	676	698	754	770	785	859	925	971	1008	1062	1124
1230	1280	1315	1359	1366	1413	1452	1465	1502	1660	1706	1914	3097	3176	3194
3312	3325	3476												

TS5

−348	43	46	67	74	174	250	290	358	387	526	551	579	608	641
680	711	768	777	851	858	890	930	1133	1160	1244	1288	1333	1369	1427
1480	1525	1644	1691	3143	3207	3255	3331	3568						

TS6

−454	51	63	74	91	108	129	174	190	233	323	341	384	498	556
568	600	640	668	773	776	844	855	911	931	988	1026	1082	1096	1190
1212	1295	1306	1342	1367	1376	1442	1525	1537	1618	1659	1754	3036	3090	3095
3141	3175	3242												

TS7

−475	55	125	149	270	341	419	505	584	624	793	870	977	1040	1049
1084	1195	1344	1360	1417	1541	1639	1718	3033	3112	3119	3228			

TS8

−2111	40	58	66	115	157	190	238	257	260	322	400	448	514	535
596	679	765	774	817	846	893	942	993	999	1010	1128	1150	1197	1216
1250	1281	1325	1352	1370	1386	1426	1476	1507	1517	1642	1718	1934	2975	3026
3095	3159	3167												

TS9

−364	41	74	112	152	221	297	372	414	466	614	650	664	760	785
835	884	1000	1013	1072	1078	1169	1185	1210	1263	1306	1349	1416	1500	1503
1622	1640	1676	3103	3117	3137	3228	3231	3495						

TS10

−1509	31	50	63	85	109	132	157	209	249	298	347	376	406	443
458	502	550	596	601	633	681	736	747	795	806	859	905	931	939
966	1011	1036	1178	1203	1265	1279	1287	1303	1314	1328	1346	1373	1379	1411
1446	1492	1501	1562	1656	1682	1776	3039	3071	3087	3175	3205			

TS11

−1485	40	80	99	144	178	213	253	293	370	432	481	495	554	610
655	679	737	803	827	904	932	966	994	1039	1043	1135	1243	1256	1271
1310	1317	1350	1373	1412	1442	1511	1572	1664	1689	1769	3016	3093	3134	3225

TS12

−923	80	119	193	226	297	397	443	539	651	670	774	797	924	955
1013	1024	1079	1101	1113	1249	1292	1348	1372	1413	1418	1474	1593	1686	1726
3054	3179	3182												

TS13

−608	143	144	266	266	314	504	505	568	777	806	806	967	1040	1042
1882	2036	2036	3389	3390	3391									

TS14

−384	53	70	140	170	238	297	301	379	405	453	577	661	681	753
773	789	843	914	947	1081	1210	1293	1309	1358	1469	1580	2024	2094	3098
3167	3334	3402												

[a] All frequencies are in cm^{-1}, and the negative numbers indicate imaginary frequencies.

TS for interconversion. The optimized structures of the decomposition products are shown in Figure 2, while the various TS are presented in Figure 3. The vibrational frequencies of all the TS are given in Table 1, while the frequencies for the reactants and stable intermediates are given in Table 2.

The potential energy profile of the unimolecular decomposition mechanism is illustrated in Figures 4, 5, and 6. The optimized geometries (XYZ coordinates) of all the reactants, products, intermediates, and TS are included as supplementary information (Tables S1−S11).

TABLE 2: Calculated Frequencies of the Intermediates and Some Important Products at the B3LYP/6-31G(d) Level of Theory

RDR

28	57	90	108	122	241	324	341	381	409	442	528
587	640	650	749	754	779	854	867	876	891	929	954
970	1133	1173	1206	1246	1249	1300	1318	1340	1342	1383	1400
1409	1461	1463	1484	1659	1679	2959	2964	3074	3142	3145	3215

RDRO

51	64	69	78	94	115	182	222	258	345	397	444
463	506	597	607	675	697	758	780	849	853	942	956
989	1000	1079	1156	1212	1220	1304	1332	1353	1368	1387	1417
1462	1488	1519	1634	1658	1758	3070	3077	3087	3131	3149	3170

INT176

60	65	73	90	101	157	200	239	268	339	413	420
496	607	608	632	662	687	757	764	778	867	898	930
950	1026	1100	1113	1163	1226	1320	1339	1352	1372	1405	1418
1454	1471	1501	1666	1700	1863	3070	3085	3094	3163	3166	3451

INT149

56	77	89	135	210	248	345	374	402	431	447	591
597	614	663	678	751	779	853	915	948	1047	1129	1239
1259	1316	1362	1404	1414	1447	1455	1484	1629	1696	3133	3199
3233	3370	3554									

INT102

13	84	165	260	296	455	532	633	672	800	869	877
989	1073	1081	1224	1286	1337	1372	1492	1516	1624	1741	3041
3088	3092	3175									

INT130

82	112	164	208	262	364	386	510	537	603	682	757
816	939	943	986	1023	1028	1058	1165	1196	1223	1255	1286
1342	1372	1417	1438	1514	1522	1543	1634	1752	2963	3021	3105
3146	3149	3597									

INT175

40	64	79	101	149	250	349	366	407	453	485	549
582	638	674	736	753	816	859	913	926	937	971	996
1064	1180	1206	1275	1286	1305	1342	1345	1383	1388	1425	1489
1508	1670	1682	1729	3060	3074	3166	3216	3220			

INT128

64	111	166	259	340	391	547	588	606	697	736	832
908	936	991	996	1051	1084	1126	1268	1273	1317	1378	1408
1438	1528	1631	1673	1716	3047	3081	3179	3221			

TAZ

353	353	689	689	755	936	1009	1030	1030	1151	1187	1196
1196	1406	1444	1444	1602	1602	3175	3175	3181			

MNH

159	269	307	334	576	587	685	686	917	1143	12330	1331
1435	1474	1671	3230	3368	3599						

MN

34	398	523	553	633	828	870	1080	1181	1349	1424	1683
1718	3126	3236									

CH$_2$NCHNH

123	378	627	633	911	979	1068	1087	1208	1301	1437	1505
1700	1728	2950	3004	3167	3436						

Here and in the discussion, the energies are corrected for ZPE. In discussions, where this correction is *not* made, we will indicate so by adding: (no ZPE).

III.A. Equilibrium Structure of RDX. The various ring conformations of RDX have been studied extensively, with detailed reviews in two recent theoretical papers.[22,23] Our predictions are quite similar to these earlier calculations and will not be discussed in detail.

The triaxial chair (AAA) with C_{3V} symmetry is the global minima, which agrees well with the earlier theoretical results[22,23] and the gas-phase electron diffraction structure.[31] We find short (2.22 Å) (N−O....H−C) H-bond intramolecular contacts that might aid the intramolecular H-transfer required for a HONO elimination primary dissociation pathway (also pointed out by Harris and Lammertsma[22]).

The tri-equatorial chair conformer (EEE) is also found to be a local minima, but it is 4.7 kcal/mol less stable than AAA.

We find that the AAA-boat conformer of RDX (see Figure 1) is 0.75 kcal/mol (no ZPE) above the AAA-chair conformation, but it has one small imaginary frequency (24i cm^{-1}), indicating that AAA-boat is *not* a stable structure for RDX (at this level of theory). Starting from this structure and minimizing the energy along this negative eigenvalue leads to the non symmetric twist boat conformer. We attempted to locate the TS corresponding to the boat to AAA chair interconversion. However, the TS converged to a higher order saddle point with two imaginary frequencies (134i and 10i cm^{-1}). The 10i cm^{-1} mode also corresponds to the boat to twist boat interconversion. Thus, the energy barrier for boat to AAA-chair interconversion is 4.3 kcal/mol (no ZPE correction).

On the basis of RHF/6-31G* calculations, Harris and Lammertsma[22] reported that the boat form of RDX is a stable minima. Using the B3LYP/6-311G**//B3LYP/6-31G* level they predict that the boat form of RDX is higher than the AAA
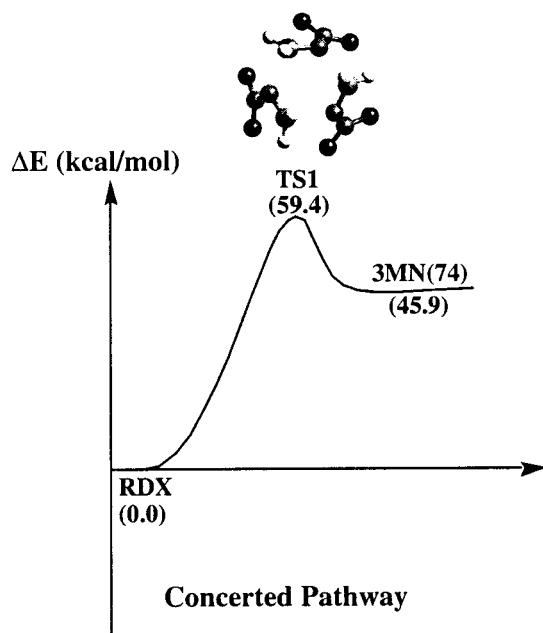
Mechanism for Unimolecular Decomposition of RDX

J. Phys. Chem. A, Vol. 104, No. 11, 2000 **2267**

Figure 4. Potential energy profile for the concerted decomposition of RDX.

chair by 0.67 kcal/mol (no ZPE) which agrees very well with our calculated ΔE of 0.75 kcal/mol (no ZPE). The structure of the boat conformer appears to be similar for both calculations.

III.B. Reaction Pathway 1. The Concerted Ring Fission. As mentioned above, the experiments by ZHL[16] were interpreted in terms of concerted ring breaking as the primary decomposition path of RDX.

For this process we computed a TS at 59.4 kcal/mol and a reaction ΔH of 45.9 kcal/mol, as shown in Figure 4. The transition structure (denoted TS1) was located by first scanning the reaction path assuming a symmetric structure, followed by optimizing the maximum energy structure along the reaction path. Then starting with this structure we found the closest saddle point (one negative eigenvalue). We did *not require* TS1 to retain the C_{3V} symmetry of RDX. At TS1 the breaking C−N bonds are ∼2.07 Å (1.460 Å is equilibrium) while all other C−N bonds (∼1.31 Å) retain character between the C−N single bond (∼1.46 Å) and double bond (∼1.26 Å), as expected. At TS1 all three fragment MN molecules have the nearly planar configuration expected for the free molecule (shown in Figure 3).

As discussed in Section I.B, the theoretical analyses by Thompson[25] indicated that a concerted dissociation cannot be the primary decomposition channel of RDX observed experimentally by ZHL if the barrier is above 40 kcal/mol. Thus, *our result that the barrier is 59.4 kcal/mol suggests that the primary decomposition pathway involves some other process.*

Several previous theoretical studies have been carried out on the energetics of the concerted ring opening process.[26,27] The most complete predictions of the barrier were recently reported by Wu and Fried.[27] Based on an extensive series of DFT calculations with a variety of basis sets they recommended the B−PW91/cc-PVDZ level of theory. This leads to E_{act} = 55.4 and ΔH = 44.6 kcal/mol (including ZPE) as compared to our results of 59.4 and 45.9 kcal/mol at the B3LYP/6-31G(d) level. (Further, ref 27 quotes E_{act} = 52.5 and ΔH = 41.8 kcal/mol rather than 55.4 and 44.6 kcal/mol. They inform us (private communication) that there was a misprint in their paper and that they agree with our results.)

III.C. Reaction Path 2. Homolytic N−N Bond Fission plus Subsequent Decomposition. *III.C.A. N−NO₂ Homolysis to Form RDR.* Since homolytic cleavage of single bonds generally do not have appreciable reverse barriers, the first N−NO₂ bond breaking in RDX[21,27] has long been considered to be a likely low-energy decomposition channel.

We calculated an N−N bond dissociation energy of 39.0 kcal/mol (including ZPE). Since the N−N bond energy for RDX is 20 kcal/mol lower than the concerted mechanism, it is plausible that initiation of the RDX decomposition occurs through the N−N bond dissociation.

The calculated N−N bond dissociation energy of RDX is slightly higher than the N−N bond in MN (see Figure 2) of 35.9 kcal/mol (including ZPE) at the G2M level of theory (B3LYP leads to 30.0 kcal/mol).[32] The estimated N−N bond dissociation energy [at the B3LYP/6-311G(d,p)//B3LYP/6-31G-(d) level with scaled HF/6-31G(d) ZPE correction] in related nitramines are 46 (dimethylnitramine), 48 (1-nitropiperidine), and 49 (1-nitro-1,3,5-triazine) (where in each case 6 kcal/mol was added to correct the energy for expected error).[22]

Starting from the pioneering work of Melius and Binkley,[21] predicted values of the N−N bond dissociation energy of RDX have ranged from 35 to 48 kcal/mol. The most recent studies predicted N−N bond dissociation energies of 34.2 (Wu and Fried[27]) and 42.0 kcal/mol (Harris and Lammertsma[22]). The 42.0 kcal/mol dissociation energy recommended by Harris and Lammertsma, included a correction of +6.0 kcal/mol based on the predicted underestimation of C−N bond energies by similar DFT calculations on related small molecules compared to much more accurate G2 energies.

Although there is some uncertainty in the exact numbers, all reliable calculations indicate that the N−N bond cleavage is ∼20 kcal/mol *more favorable* than the concerted ring fission.

III.C.B. Subsequent Decomposition of RDR. The RDR radical formed after the elimination of first NO₂ can undergo further decomposition through two distinct reaction channels as shown in Figure 5. The possibility of other decomposition channels from RDR cannot be ruled out, but we find that the two reaction paths presented here are energetically the most favorable. Melius and Binkley proposed several possible decomposition schemes from RDR,[21] including these two.

The minimum energy conformation of RDR has the N-radical center between a planar (half chair) and a nonplanar (chair) conformation (see Figure 2). The N radical in RDR is known[22] to hyperconjugate with the neighboring C−H hydrogens, providing extra stability to the radical and weakening the bond.

III.C.B.1. The Ring Opening Pathway for RDR Decomposition. III.C.B.1a. Formation of RDR-o + NO₂. The most commonly considered decomposition pathway is the opening of the RDR ring.[21] We also find ring opening of the radical to be the least energy pathway, requiring an additional 26.4 kcal/mol energy. The ring opened structure (RDR-o) is 13.5 kcal/mol less stable than RDR. Two additional possible pathways are concerted ring fission and HONO elimination from RDR. However, our analysis of the product energies confirmed that these two processes cannot compete with the ring opening channel.

The ring opening of RDX preferably occurs through the breaking of the C−N bond between the C atom adjacent to the radical center and its next nitrogen atom. TS2 was generated by first scanning the dissociating C−N bond to find a candidate TS. The C−N bond was varied from 1.5 to 2.4 Å with an interval of 0.1 Å, and each point along the reaction coordinates was then optimized fully (except the reaction coordinate). The
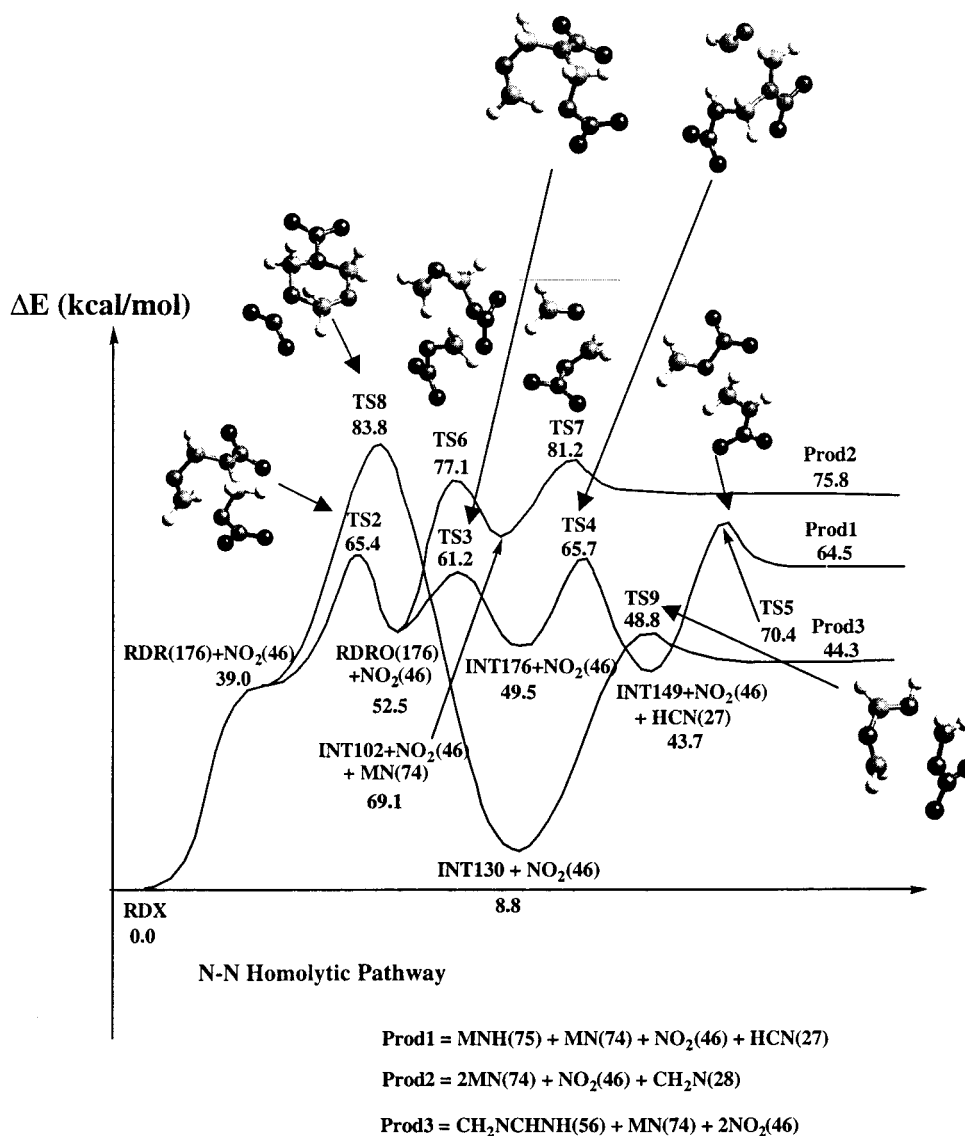
Figure 5. Potential energy profile for the N−N bond cleavage and the following decomposition of the radical.

maximum, centered around 2.1 Å, was then fully optimized (requiring a single negative curvature) to locate saddle point TS2. To locate the minimum energy structure of RDR-o, we started with the optimized structure at 2.4 Å from the scan and then optimized it fully, which leads to an optimized structure for RDR-o with the nonbonded C−N bond at 3.448 Å. This confirms that TS2 properly connects RDR and RDR-o.

III.C.B.1b. Decomposition of RDR-o by H Migration Followed by CN Elimination. A close look at the reaction path from TS2 to RDR-o, reveals that as the C−N bond moves further along the reaction path, the CH_2 rotates so that the H-atoms approach the breaking N-atom, as shown in Figure 3, leading to a nonbonded contact of 2.798 Å between the H and N atom in RDR-o. Indeed, we find that the least energy pathway for decomposition of RDR-o involves H-migration through TS3. The barrier to H-migration is only 8.7 kcal/mol at TS3, and the isomeric product INT176 is 3.0 kcal/mol more exothermic than RDR-o.

We searched for a TS for possible elimination of CH_2N radical from RDR-o, but these calculations always led to H-migration (because of the favorable N−H nonbonded contact in RDR-o).

III.C.B.1c. Decomposition of INT176 (isomer of RDR-o). INT176, which is an isomer of RDR and RDR-o, can eliminate

HCN to form INT149 (a stable radical intermediate) via TS4, which has a barrier of 16.2 kcal/mol with respect to INT176. The structure of INT149 can be visualized as the result of bonding the MN molecule to the CH_2NHNNO_2 (MNH) radical. The C−N bond of the MN fragment in INT149 has partial double bond character (1.367 Å), whereas the C−N bond in the MNH fragment (1.440 Å) and the C−N bond joining the two moieties (1.470 Å) have single bond character. Thus, INT149 can easily fission to form MN and MNH radical by breaking the common C−N bond, the barrier (TS5) of which is 26.7 kcal/mol above INT149. The product MNH has C−N and N−N bond lengths of 1.362 and 1.381 Å, respectively, with the radical character centered around the central N-atom.

III.C.B.1d. MN and MNH Decomposition. The structure of MN is well-known theoretically.[33,34] The decomposition pathways of MN (CH_2NNO_2) are N−NO_2 cleavage, HCN + HONO formation, and H_2CO + N_2O formation. ZHL reported HONO formation as the dominant secondary decomposition channel, but recent theoretical results support N−N bond breaking as the rate-limiting process.[32,34]

MNH may also decompose in a similar manner either to CH_2-NH + NO_2, CH_2N + HONO, or simple H-elimination to MN and H. We did not examine these secondary decomposition paths in the present study.

Mechanism for Unimolecular Decomposition of RDX

J. Phys. Chem. A, Vol. 104, No. 11, 2000 **2269**

III.C.B.1e. The Concerted Pathway for RDR-o Decomposition. We searched for a concerted decomposition of RDR-o to two MN and CH$_2$N, but this did not converge to a reliable TS. Rather we found a stepwise mechanism for this process via TS6 and TS7 as shown in Figure 5.

RDR-o can dissociate to INT102 and MN via TS6, leading to a barrier 24.6 kcal/mol above RDR-o. INT102 can again dissociate to CH$_2$N and MN by breaking the joining C−N bond. The barrier for this process at TS7 is 20 kcal/mol. The breaking C−N bond in TS7 is 1.936 Å, and both the fragments are close to their respective minimum energy structure.

The final products of the concerted ring opening, 2CH$_2$NNO$_2$, and CH$_2$N are 36.8 kcal/mol more endothermic than RDR, as shown in Figure 5. Hence, the associated TS (TS7) is 15.8 kcal/mol higher than TS2. As will be discussed in the next section, the HONO elimination process requires a barrier of 35−40 kcal/mol so that the corresponding TS will also be much higher in energy than TS2.

III.C.B.1f. Elimination of Second NO$_2$ from RDR. The elimination of a second NO$_2$ group from RDR becomes difficult due to formation of a biradical (unpaired spin on each of the two N radical centers). This high energy conformation can be avoided by H-migration with simultaneous NO$_2$ elimination. This leads to TS8, as shown in Figure 5. As the N−NO$_2$ distance increases in TS8, the H atom from the neighboring CH$_2$ group migrates to the N-atom and the adjacent C−N bond (between the N radical in RDR and H migrating C) gains partial double bond character (1.324 Å). The breaking N−N bond in TS8 is 1.976 Å and the migrating H atom is 1.414 Å from the N and 1.270 Å from C. TS8 has a barrier of 44.8 kcal/mol over RDR and goes to a stable intermediate (INT130).

III.C.B.1g. Concerted Breaking of INT130. INT130 can further decompose concertedly to CH$_2$NCHNH ($M = 56$) and MN via TS9. The breaking CN bonds in TS9 are 2.405 and 1.941 Å, respectively. Both the fragments in TS9 are close to their respective planar structure. The geometry of the CH$_2$-NCHNH product is shown in Figure 2.

III.C.C. Summary. The three sets of products formed in the N−N homolytic pathway are represented as prod1, prod2, and prod3 in Figure 5. Although the initial dissociation of RDX to form RDR requires less energy than the concerted ring breaking process, the overall endothermicity of three sets of products (prod1, prod2, and prod3) in the former are much higher than that of the products of the concerted ring fission. Thus, an isolated energetic RDX molecule will prefer a concerted ring breaking to form three MN molecules over decomposition of the RDR to form products.

III.D. Reaction Pathway 3. The Concerted HONO Elimination. We find a third pathway, concerted HONO elimination (reaction pathway three), to be more favorable than the concerted and N−N homolytic pathways discussed above. This new pathway has not been considered in previous theoretical calculations although *m/e* 81 was experimentally observed by molecular beam[16] as well as in the pyrolysis experiments.[12,13]

Based on the close nonbonded contact of H and NO$_2$ in RDX a possibility of H migration or HONO elimination from RDX was suggested by Harris and Lammertsma.[22] We searched for a possible HONO elimination TS from RDX and found that TS10 for the first HONO elimination has a barrier of 39.2 kcal/mol (very close to the calculated N−N bond dissociation energy of 39.0 kcal/mol). Such a similarity in energy (32.7 kcal/mol for HONO elimination and 35.9 kcal/mol N−N bond dissociation) was also observed in the secondary decomposition of

MN.[32] This can be attributed to the smaller secondary C−H bond strength in nitramines compared to aliphatic or aromatic C−H bonds.[22]

For RDX this HONO pathway leads to INT175 and HONO which are 8.5 kcal/mol *exothermic* from RDX, as shown in Figure 6. The structure of TS10 is quite similar to the HONO elimination TS observed in MN[32,33] or dimethylnitramine[35] as shown in Figure 3.

III.D.1. Second HONO Elimination. INT175 can eliminate another molecule of HONO via TS11 to form INT128, leading to a TS11 energy 32.0 kcal/mol above RDX.

III.D.2. Third HONO Elimination. INT128 can subsequently eliminate another HONO molecule via TS12 to form a very stable TAZ (INT81) intermediate. TS12 has an energy of 20.1 kcal/mol with respect to RDX. Thus, the decomposition of RDX to 3 HONO + TAZ is *exothermic* by *36.4* kcal/mol. Of the various unimolecular decompositions from RDX this is the only one that is exothermic (energy released).

The breaking N−N bonds in TS10, TS11, and TS12 are 2.104, 2.123, and 2.233, and the breaking C−H bonds are 1.332, 1.324, and 1.223; whereas the forming OH bonds are 1.305, 1.318, and 1.457 and the forming CN π bonds are 1.345, 1.352, and 1.392 Å, respectively. Due to the formation of a CNπ bond via the elimination of HONO in INT175 and INT128, the neighboring NO$_2$ group rearranges from axial to equatorial orientation. INT81 has a longer CN double bond of 1.337 Å compared to INT175(1.272) and INT128(1.277, 1.285), due to the complete delocalization of the π cloud which brings a D_{3h} symmetry to the structure.

III.D.3. TAZ Concerted Decomposition. TAZ is a very stable intermediate. We find that it unzips through a concerted mechanism to three HCN, but with an energy barrier of 88.6 kcal/mol (TS13) (located in the same way as TS1). However, considering that TAZ + 3 HONO is 36.4 kcal/mol more stable than RDX, the overall energy requirement for the decomposition is 52.2 kcal/mol with respect to RDX.

The final products, 3HCN + 3HONO are 14.2 kcal/mol endothermic from RDX.

TS13 is a symmetric planar TS, with the breaking CN bonds at 1.974 Å (1.337 Å equilibrium) while the fragment HCNs are each close (H−C−N angles of 145.3°) to the product linear structure.

III.D.4. Concerted Ring Decomposition of INT175 and INT128. Concerted ring breaking of INT175 to two MN and HCN or INT128 to MN and two HCN are conceivably low energy paths for the formation of MN alternative to the concerted and N−N homolysis pathways. Consequently, we searched for possible TS from INT175 and INT128. We did not find a reliable TS from INT175. However, TS14 is a genuine TS for concerted breaking of INT128 to 2HCN and MN. TS14 has an energy of 51.7 kcal/mol above RDX. Thus, this could be considered as an additional low energy path for the formation of MN.

III.D.5. Possible Formation of OST. OST ($m/e = 97$) was observed as one of the major unimolecular decomposition products of RDX in most of the condensed phase decomposition experiments.[2,12] However, the mass fragment 97 was not detected by ZHL in their IRMPD study of isolated RDX molecule.[16] Behrens and Bulusu[2] proposed an intramolecular rearrangement mechanism for the formation of OST which involved elimination of an HNO and two HONO molecules from RDX. Since the intermediate formed after elimination of two HONO molecules (INT128) is 13.0 kcal/mol more stable than RDX in the HONO elimination pathway, we believe that
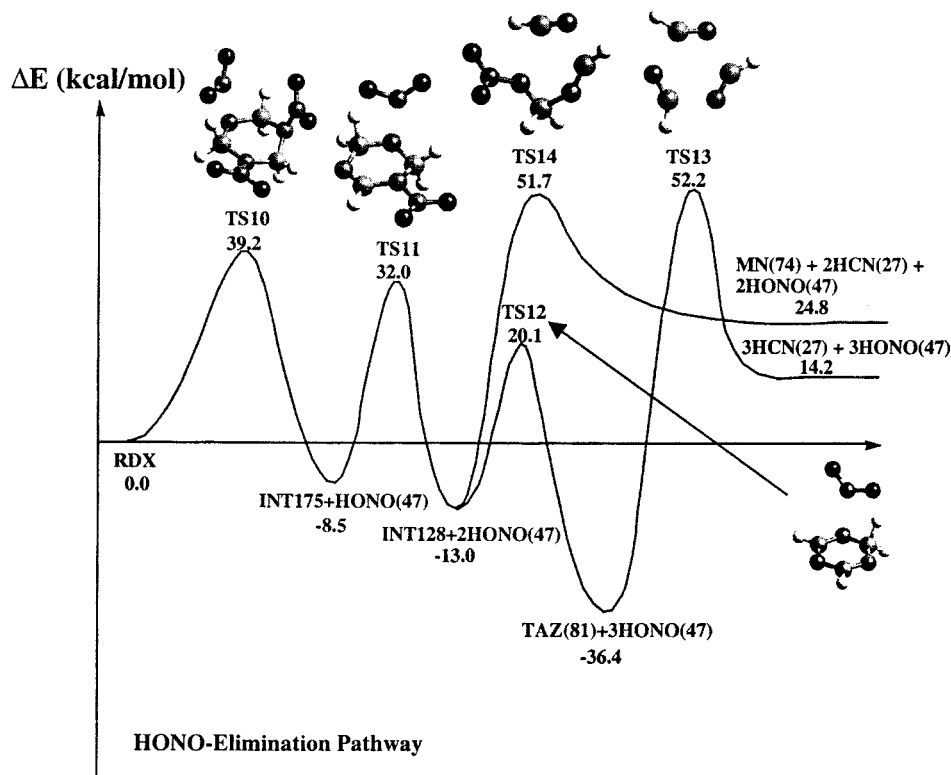
Figure 6. Potential energy profile of the concerted HONO elimination from RDX and the following decompositions.

the formation of OST will more preferably occur from INT128 via the elimination of an HNO molecule.

Behrens and Bulusu proposed that the mechanism of forming OST from INT128 involves migration of one of the CH_2 hydrogens to the oxygen atom of the neighboring NO_2 group as a first step. To test this possibility we performed a scan of the nonbonded H...O distance from INT128. As the H atom approaches the O atom of the NO_2 group, the neighboring N—N bond becomes larger and formation of a C—N π bond occurs which finally lead to the formation of TAZ + HONO. The proposed intermediate after H-migration is also found to be unstable, leading to the decomposition to TAZ + HONO when optimized fully. Since the initial H-migration preferably leads to the elimination of HONO, formation of OST cannot be explained by this mechanism.

On the other hand, our calculations do show OST + HNO + 2HONO to be energetically 6.9 kcal/mol more stable than TAZ + 3HONO. Thus we cannot deny that there might be some other unexplored mechanism for the formation of OST, perhaps a nitro—nitrite rearrangement in INT128 followed by the elimination of HNO molecule.

IV. Discussion

Comparison of Experimental Mass Spectra. Our calculations indicate that HONO elimination is the most favorable channel for RDX decomposition and it is the only channel leading to exothermic unimolecular decomposition. Beside establishing the minimum energy pathways for RDX decomposition, a complete mechanism must account for all mass fragments detected in TOFVS (ZHL)[16] and the laser pyrolysis studies.[12]

We find that the threshold for unimolecular decomposition of RDX is 40 kcal/mol which forms RDR(176) + NO_2(46) by N—N homolytic and TAZ(81) + 3HONO(47) by HONO elimination.

With a total energy of ~52 kcal more, we expect to see decomposition of TAZ to form 3HCN(27) plus decomposition of INT128 to form MN(74) and 2 HCN(27). Furthermore, at an energy of ~50 kcal/mol, we expect decomposition of HONO to OH(17) and NO(30).

With a total energy of ~60 kcal/mol we expect opening of the concerted pathway to form 3 MN(74).

With ~70 kcal/mol we expect RDR decomposition to form MNH(75), MN(74), and HCN(27) to become possible.

Finally, with ~80 kcal/mol or above, RDR decomposition through another two channels (see Figure 5) opens up and it becomes possible to form MN(74) and CH_2N(28) via decomposition of INT102, and to form CH_2NCHNH(56), MN(74), and NO_2(46) via INT130.

This leads to the schematic diagram for mass fragments from decomposing RDX at different internal energy as shown in Figure 7. Given the total internal energy of 80 kcal/mol for RDX molecule in the ZHL laser studies, all the three above channels might be energetically accessible. The major mass fragments detected by ZHL are 120, 102, 81, 74, 56, 46, 44, 42, 26−30, and 12−17. At around 40 kcal/mol energy the only mass fragments which could be found are 176(INT176), 81(INT81), 47(HONO), and 46(NO_2). 176 is a result of N—N bond homolytic cleavage and was evident in most of the experiments.[16-20.] The mass 81, which is a major decomposition product found at this energy, was observed as a strong peak by ZHL[16] and also by others.[12,13] On the basis of their translational energy distributions, ZHL considered mass 81 as a faster decomposition component of mass 176. Our calculation clearly indicates that this is *not* the case, mass 81 could be formed directly through consecutive HONO elimination (pathway 3). INT175 and INT128 are short-lived intermediates, and hence, these mass fragments are not likely to be observed experimentally.

There was no evidence of m/e 47(HONO) in the IRMPD study of ZHL because it undergoes further decomposition to

Mechanism for Unimolecular Decomposition of RDX

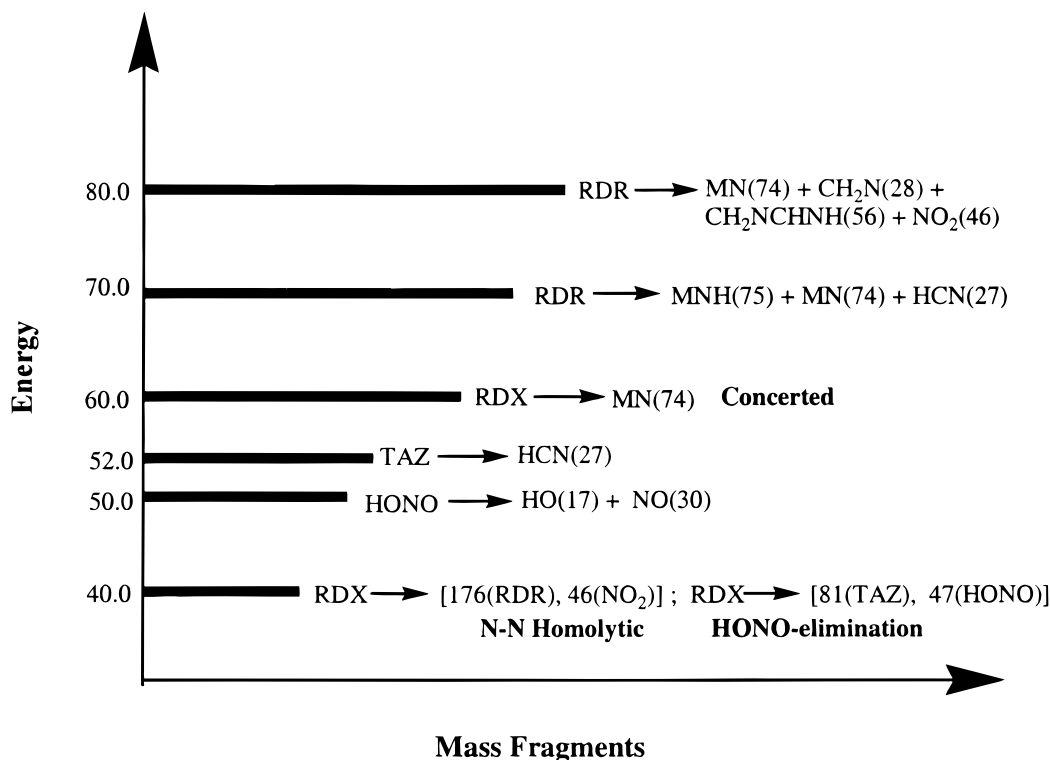*J. Phys. Chem. A, Vol. 104, No. 11, 2000* **2271**

Figure 7. Schematic diagram of the decomposing mass fragments at different internal energy.

OH(17) and NO(30) with a barrier of 49.6 kcal/mol (calculated). This is consistent with a recent pyrolysis study of Lee et al.,[12] who observed m/e 47 as a parent mass peak (with m/e 17 observed experimentally mainly due to decomposition of HONO).[16,17] However, in ref 16, ZHL observed only a slower component of OH generated from the decomposition of secondary HONO obtained from CH_2NNO_2 (MN) decomposition.

At around 52 kcal/mol energy we expect 27(HCN) to be found while at 60 kcal/mol we expect 74(MN) to be formed in addition to the lower energy products. Indeed, 74 was observed as a major mass fragment experimentally.[16] With ~52 kcal/mol we find m/e 74 can be formed through the HONO elimination channel. The faster component of 74 observed by ZHL was considered to be the result of the decomposition of parent RDX molecule through concerted ring breaking. When the internal energy of the molecule is around 60 kcal/mol, reaction path 1 is accessible, which justifies the fast component of 74 found experimentally.

At an energy of 70−80 kcal/mol the RDR decomposition from N−N homolysis pathway is also accessible which could form the mass fragments 75(MNH), 74(MN), 27(HCN), and 102(INT102). However, RDR-o, INT176, and INT149 are not very stable intermediates and might not be observed experimentally.

We calculate that at 81 to 84 kcal/mol the decomposition of INT102 and INT130 (see Figure 5) would lead to mass fragments 74(MN), 28(CH_2N), and 56(CH_2NCHNH). Since the energetics may be off by ~3 kcal/mol they might also be accessible by the ZHL experiments.

Our calculations account for all mass fragments (including m/e 102, 81, 74, 56, 46, 30, 27, and 17) observed by ZHL in their IRMPD study except for m/e 120, which is not a major product. The possible formula of $CH_2N_3O_4$ was suggested by ZHL for m/e 120, who considered it as decomposition product of 176(RDR). However, we have not found a rearrangement pathway from RDR leading to formation of 120. Thus, we

cannot understand how 120 could result from a primary decomposition pathway.

The other smaller mass fragments observed experimentally by ZHL, such as 44(N_2O), 29(H_2CO), etc., result from secondary decomposition of such products as MN. At around 33 kcal/mol energy MN can decompose to 47(HONO) and 27(HCN) whereas ~38 kcal/mol energy is required to form 44(N_2O) and 29(H_2CO).[32] Thus, the (74) MN resulting from the HONO elimination pathway can undergo further decomposition at an energy ~60 kcal/mol while, ~80 kcal/mol or higher energy is required for the secondary decomposition of MN formed via the other two pathways.

V. Summary

Our calculations lead to the following conclusions about RDX decomposition:

(i) Three distinct reaction pathways are identified for the unimolecular decomposition of RDX. The consecutive HONO elimination to form TAZ and 3HONO (with further decomposition of TAZ to 3HCN) is identified as the energetically most favorable decomposition pathway. N−N bond cleavage to form RDR is also favorable but the associated endothermicity for further decomposition makes this channel less favorable than the other two reaction paths.

(ii) The present scheme successfully accounts for the mass fragments observed in molecular beam experiments except for m/e 120.

(iii) The HONO elimination reaction pathway is the most exothermic primary decomposition channel and may account for the energy release observed in the decomposition of RDX. Of course, most of the energy released in the gas-phase comes from secondary reactions.

Supporting Information Available: Tables S1−S11 contain the optimized geometries (XYZ coordinates) of all the reactants, products, intermediates, and TS. This material is available free of charge via the Internet at http://pubs.acs.org.

References and Notes

(1) Adams, G. F.; Shaw, R. W., Jr. *Annu. Rev. Phys. Chem.* **1992**, *43*, 311.

(2) (a) Behrens, R., Jr.; Bulusu, S. *J. Phys. Chem.* **1992**, *96*, 8877, 8891. (b) Behrens, R., Jr.; Bulusu, S. *J. Phys. Chem.* **1991**, *95*, 5838. (c) Behrens, R., Jr. *J. Phys. Chem.* **1990**, *94*, 6706. (d) Behrens, S., Jr. In *Chemistry and Physics of Energetic Materials*; Bulusu, S. N., Ed.; Kluwer: Dordrecht, 1990; p 347.

(3) Rauch, F. C.; Fanelli, A. J. *J. Phys. Chem.* **1969**, *73*, 1604.

(4) Batten, J. J. *Aust. J. Chem.* **1974**, *24*, 945.

(5) Cosgrove, J. D.; Owen, A. J. *Combust. Flame* **1974**, *22*, 13.

(6) Farber, M.; Srivastave, R. D. *Chem. Phys. Lett.* **1979**, *64*, 307.

(7) Doyle, R. J., Jr.; Campana, J. E. *J. Phys. Chem.* **1985**, *89*, 4251.

(8) Hoffsommer, J. C.; Glover, D. J. *Combust. Flame* **1985**, *59*, 303.

(9) Oxens, F. J.; Sharma, *J. Appl. Phys.* **1980**, *51*, 1494.

(10) Bulusu, S.; Weinstein, D. I.; Autera, J. R.; Velicky, R. W. *J. Phys. Chem.* **1986**, *90*, 4121.

(11) Brill, T. B.; Gongwer, P. E.; Williams, G. K. *J. Phys. Chem.* **1994**, *98*, 12242.

(12) Lee, Y.; Tang, C.-J.; Litzinger, T. A. *Combust. Flame* **1999**, *117*, 600.

(13) Ermolin, N. E.; Zarko, V. E. *Combust. Explosion Shock Waves* **1997**, *33*, 251.

(14) Rogers, R. N.; Daub, G. W. *Anal. Chem.* **1973**, *45*, 596.

(15) Zuckermann, H.; Greenblatt, G. D.; Haas, Y. *J. Phys. Chem.* **1987**, *91*, 5159.

(16) Zhao, X.; Hinsta, E. J.; Lee, Y. T. *J. Chem. Phys.* **1988**, *88*, 801.

(17) Capellos, C.; Papagiannakopulous, P.; Liang, Y.-L. *Chem. Phys. Lett.* **1989**, *164*, 533.

(18) Botcher, T. R.; Wight, C. A. *J. Phys. Chem.* **1994**, *98*, 5441; **1993**, *97*, 9149.

(19) Pace, M. D. *J. Phys. Chem.* **1991**, *95*, 5858.

(20) Choi, M.; Kim, H.; Chung, C. *J. Phys. Chem.* **1995**, *99*, 15785.

(21) (a) Melius, C. F.; Binkley, J. S. *Symp. (Int.) Combust., [Proc.], 21st* **1986**, 1953. (b) Melius, C. F. In *Chemistry and Physics of Energetic Materials;* Bulusu, S. N., Ed.; Kluwer: Dordrecht, 1990; p 21.

(22) Harris, N. J.; Lammertsma, K. *J. Am. Chem. Soc.* **1997**, *119*, 6583.

(23) Rice, B. M.; Chabalowski, C. F. *J. Phys. Chem. A.* **1997**, *101*, 8720.

(24) Sewell, T. D.; Thompson, D. L. *J. Phys. Chem.* **1991**, *95*, 6228.

(25) Chambers, C. C.; Thompson, D. L. *J. Phys. Chem.* **1995**, *99*, 15881.

(26) Habibollahzadeh, D.; Grodzicki, M.; Seminario, J. M.; Politzer, P. *J. Phys. Chem.* **1991**, 95, 7699.

(27) Wu, C. J.; Fried, L. E. *J. Phys. Chem. A.* **1997**, *101*, 8675.

(28) Becke, A. D. *J. Chem. Phys.* **1993**, *98*, 5648, 1372; **1992**, *96*, 2155; **1992**, *97*, 9173.

(29) Lee, C.; Yang, W.; Parr, R. G. *Phys. Rev. B.* **1988**, *37*, 785.

(30) (a) Jaguar 3.5; Schrödinger Inc.: Portland, OR, 1998. (b) Greeley, B. H.; Russo, T. V.; Mainz, D. T.; Friesner, R. A.; Langlois, J−M.; Goddard, W. A., III; Donnelly, R. E.; Ringnalda, M. N. *J. Chem. Phys.* **1994**, *101*, 4028.

(31) (a) Shishkov, I. F.; Vilkov, L. V.; Kolonits, M.; Rozsondai, B. *Struct. Chem.* **1991**, *2*, 57. (b) Choi, C. S.; Prince, E. *Acta Crystallogr.* **1972**, *B28*, 2857.

(32) Chakraborty, D.; Lin, M. C. Gas-Phase Chemical Kinetics of [C, H, N, O]-Systems Relevant to the Combustion of Nitramines in Their Early Stages. *J. Prop. Power,* in press.

(33) Mowrey, R. C.; Page, M.; Adams, G. F.; Lengsfield, B. H., III. *J. Chem. Phys.* **1990**, *93*, 1857.

(34) Rice, B. M.; Adams, G. F.; Page, M.; Thompson, D. L. *J. Chem. Phys.* **1995**, *99*, 5016.

(35) Harris, N. J.; Lammertsma, K. J. *J. Phys. Chem. A.* **1997**, *101*, 1370.